Hindawi
Mathematical Problems in Engineering
Volume 2017, Article ID 3804751, 12 pages
https://doi.org/10.1155/2017/3804751

Research Article

The Influence of Slip Boundary Condition on Casson Nanofluid Flow over a Stretching Sheet in the Presence of Viscous Dissipation and Chemical Reaction

Ahmed A. Afify[1,2]

[1]*Department of Mathematics, Deanship of Educational Services, Qassim University, P.O. Box 6595, Buraidah 51452, Saudi Arabia*
[2]*Department of Mathematics, Faculty of Science, Helwan University, P.O. Box 11795, Ain Helwan, Cairo, Egypt*

Correspondence should be addressed to Ahmed A. Afify; afify65@yahoo.com

Received 2 March 2017; Revised 19 May 2017; Accepted 30 May 2017; Published 26 July 2017

Academic Editor: Efstratios Tzirtzilakis

The impacts of multiple slips with viscous dissipation on the boundary layer flow and heat transfer of a non-Newtonian nanofluid over a stretching surface have been investigated numerically. The Casson fluid model is applied to characterize the non-Newtonian fluid behavior. Physical mechanisms responsible for Brownian motion and thermophoresis with chemical reaction are accounted for in the model. The governing nonlinear boundary layer equations through appropriate transformations are reduced into a set of nonlinear ordinary differential equations, which are solved numerically using a shooting method with fourth-order Runge-Kutta integration scheme. Comparisons of the numerical method with the existing results in the literature are made and an excellent agreement is obtained. The heat transfer rate is enhanced with generative chemical reaction and concentration slip parameter, whereas the reverse trend is observed with destructive chemical reaction and thermal slip parameter. It is also noticed that the mass transfer rate is boosted with destructive chemical reaction and thermal slip parameter. Further, the opposite influence is found with generative chemical reaction and concentration slip parameter.

1. Introduction

Nowadays, nanofluids have been utilized as the working fluids instead of the base fluids due to their high thermal conductivity. Choi [1] is the first researcher who established fluids containing a suspension of nanosize particles which are termed the nanofluids. Lee et al. [2] confirmed that the nanofluids possess outstanding heat transfer characteristics compared to those of base fluids. Later on, many investigators [3–7] have indicated that the nanofluids enhanced thermophysical characteristics and heat transfer behavior compared to the base fluids. The thermal conductivity enhanced by 40% when copper nanoparticles with the volume fraction less than 1% are added to the ethylene glycol or oil was studied by Eastman et al. [3]. The enhancement of thermal conductivity of various nanofluids was reviewed by Aybar et al. [4]. They confirmed that the addition of nanoparticles in the fluids increases the thermal conductivity. Wang et al. [5] discussed the viscosity of Al2O3 and CuO nanoparticles dispersed in water, vacuum pump fluid, engine oil, and ethylene glycol. Their results indicated that 30% enhancement with Al2O3/water nanofluid at 3% volume concentration is obtained. Afify and Bazid [6] investigated the impacts of variable viscosity and viscous dissipation on the boundary layer flow and heat transfer along a moving permeable surface immersed in nanofluids. The influences of thermal radiation and particle shape on the Marangoni boundary layer flow and heat transfer of nanofluid driven by an exponential temperature were examined by Lin et al. [7].

Buongiorno, [8] modified the reasons behind the enhancement of heat transfer of nanofluids. Recently, many researchers [9–15] have effectively applied Buongiorno's model [8]. Nield and Kuznetsov [9] presented the influence of Brownian motion and thermophoresis on natural convection boundary layer flow past a vertical plate suspended in a porous medium. The steady two-dimensional boundary layer flow of a nanofluid past a stretching surface was examined by Khan and Pop [10]. Nield and Kuznetsov [11] discussed

the impact of Brownian motion and thermophoresis on the double-diffusive nanofluid convection past a vertical plate embedded in a porous medium. Makinde and Aziz [12] discussed the influence of a convective boundary, Brownian motion, and thermophoresis on the steady two-dimensional boundary layer flow of a nanofluid past a stretching sheet. Rana et al. [13] numerically examined the Brownian motion and thermophoresis effects on the steady mixed convection boundary layer flow of nanofluid past an inclined plate embedded in a porous medium. The influence of variable fluid properties with Brownian motion and thermophoresis on the natural convective boundary layer flow in a nanofluid past a vertical plate was numerically studied by Afify and Bazid [14]. Recently, Makinde et al. [15] numerically examined the effects of variable viscosity, thermal radiation, and magnetic field on convective heat transfer of nanofluid over a stretching surface.

Non-Newtonian nanofluids are widely encountered in many industrial and technological applications, such as the dissolved polymers, biological solutions, paints, asphalts, and glues. The power-law non-Newtonian nanofluid along a vertical plate and a truncated cone saturated in a porous medium were analyzed by Hady et al. [16] and Cheng [17], respectively. Rashad et al. [18] investigated the natural convection of non-Newtonian nanofluid around a vertical permeable cone. The influence of Soret and Dufour on the mixed convective flow of Maxwell nanofluid over a permeable stretched surface was examined by Ramzan et al. [19]. Several authors [20–23] have analytically solved the problem of non-Newtonian nanofluids in various aspects using the homotopy analysis method (HAM). Abou-Zeid et al. [24] examined the impact of viscous dispersion on the mixed convection of gliding motion of bacteria on power-law nanofluids through a non-Darcy porous medium. The influence of nonuniform heat source/sink with the Brownian motion and thermophoresis on non-Newtonian nanofluids over a cone was illustrated by Raju et al. [25].

The Casson fluid model is classified as a subclass of non-Newtonian fluid which has several applications in food processing, metallurgy, drilling operations, and bioengineering operations. The Casson fluid model was discovered by Casson in 1959 for the prediction of the flow behavior of pigment-oil suspensions [26]. Boundary layer flow of Casson fluid and Casson nanofluid flow over different geometries was considered by many authors [27–30]. Mustafa et al. [27] analytically discussed the unsteady boundary layer flow of a Casson fluid over a moving flat plate using the homotopy analysis method (HAM). Nadeem et al. [28] examined the analytical solution of convective boundary conditions for the steady stagnation-point flow of a Casson nanofluid. Makanda et al. [29] studied the numerical solution of MHD Casson fluid flow over an unsteady stretching surface saturated in a porous medium with a chemical reaction effect. Recently, Hayat et al. [30] investigated the combined effects of the variable thermal conductivity and viscous dissipation on the boundary layer flow of a Casson fluid due to a stretching cylinder.

The chemical reaction influence is a significant factor in the study of heat and mass transfer for many branches of science and engineering. A chemical reaction between the base liquid and nanoparticles may regularly occur either throughout a given phase (homogeneous reaction) or in an enclosed region (boundary) of the phase (heterogeneous reaction). Das et al. [31] investigated numerically the effects of chemical reaction and thermal radiation on the heat and mass transfer of an electrically conducting incompressible nanofluid over a heated stretching sheet. The effect of time-dependent chemical reaction on stagnation-point flow and heat transfer of nanofluid over a stretching sheet was presented by Abd El-Aziz [32]. El-Dabe et al. [33] studied the impact of chemical reaction, heat generation, and radiation on the MHD flow of non-Newtonian nanofluid over a stretching sheet embedded in a porous medium. Eid [34] proposed the numerical analysis of MHD mixed convective boundary layer flow of a nanofluid through a porous medium along an exponentially stretching sheet in the presence of chemical reaction and heat generation or absorption effects. Recently, Afify and Elgazery [35] discussed the influences of the convective boundary condition and chemical reaction on the MHD boundary layer flow of a Maxwell nanofluid over a stretching surface.

All these previous studies restricted their discussions on conventional no-slip boundary conditions. However, both velocity slip and temperature jump at the wall have numerous benefits in many practical applications such as micro- and nanoscale devices. In 1823, Navier [36] became the first person to create the slip boundary condition and suggested that the slip velocity is linearly proportional to the shear stress at the wall. Following him, many researchers [37–42] have widely studied the velocity slip and temperature jump at the wall over various geometries placed in viscous fluids and nanofluids. The impacts of slip and convective boundary condition on the unsteady three-dimensional flow of nanofluid over an inclined stretching surface embedded in a porous medium were numerically discussed by Rashad [37]. Afify et al. [38] used Lie symmetry analysis to investigate the effects of slip flow, Newtonian heating, and thermal radiation on MHD flow and heat transfer along the permeable stretching sheet. EL-Kabeir et al. [39] examined the numerical solution for mixed convection boundary layer flow of Casson non-Newtonian fluid about a solid sphere in the presence of thermal and solutal slip conditions. Afify [40] examined the impact of slips and generation/absorption on an unsteady boundary layer flow and heat transfer over a stretching surface immersed in nanofluids. Abolbashari et al. [41] presented an analytical solution to analyze the heat and mass transfer characteristics of Casson nanofluid flow induced by a stretching sheet with velocity slip and convective surface boundary conditions. Recently, Uddin et al. [42] discussed the effects of Navier slip and variable fluid properties on the forced convection of nanofluid and heat transfer over a wedge. The objective of the present paper is to investigate the influences of chemical reaction, viscous dissipation, velocity, and thermal and concentration slip boundary conditions in the presence of nanoparticles attributable to Brownian diffusion and thermophoresis on flow and heat transfer of Casson fluid over a stretching surface. To the best of the author's knowledge, this work has not been previously studied in the scientific research. Numerical

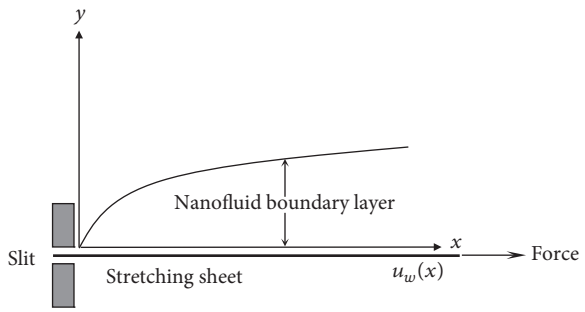

Figure 1: Physical model and coordinate system.

results for the velocity, temperature, and nanoparticle concentration fields are plotted. The friction factor and the heat and mass transfer rates are also tabulated and discussed. The present paper confirmed that the nanoparticles embedded in Casson fluid have many practical applications such as nuclear reactors, microelectronics, chemical production, and biomedical fields.

2. Mathematical Formulation

Consider the steady boundary layer flow of an incompressible Casson nanofluid past a stretching surface. The sheet is stretched with a linear velocity $u_w(x) = bx$, where b is the positive constant. The x-axis is directed along the continuous stretching sheet and the y-axis is measured normal to the x-axis. It is assumed that the flow takes place for $y > 0$. The temperature and the nanoparticle concentration are maintained at prescribed constant values T_w, C_w at the surface and T_∞ and C_∞ are the fixed values far away from the surface. It is also assumed that there is a first-order homogeneous chemical reaction of species with reaction rate constant, K_0. The flow configuration is shown in Figure 1. The rheological equation of state for an isotropic and incompressible flow of Casson fluid is given by Eldabe and Salwa [43]:

$$\tau_{ij} = \begin{cases} 2\left(\mu_B + \dfrac{p_y}{\sqrt{2\pi}}\right)e_{ij}, & \pi > \pi_c, \\ 2\left(\mu_B + \dfrac{p_y}{\sqrt{2\pi_c}}\right)e_{ij}, & \pi < \pi_c, \end{cases} \tag{1}$$

where μ_B is the plastic dynamic viscosity of the non-Newtonian fluid, p_y is the yield stress of fluid, π is the product of the component of deformation rate and itself, namely, $\pi = e_{ij}e_{ij}$, e_{ij} is the (i, j) component of the deformation rate, and π_c is a critical value of π based on non-Newtonian model. Under the boundary layer approximations the governing equations of Casson nanofluid can be expressed as follows (Buongiorno [8] and Haq et al. [44]):

$$\frac{\partial u}{\partial x} + \frac{\partial v}{\partial y} = 0, \tag{2}$$

$$u\frac{\partial u}{\partial x} + v\frac{\partial u}{\partial y} = \upsilon\left(1 + \frac{1}{\beta}\right)\frac{\partial^2 u}{\partial y^2}, \tag{3}$$

$$u\frac{\partial T}{\partial x} + v\frac{\partial T}{\partial y} = \alpha\frac{\partial^2 T}{\partial y^2} + \tau\left\{D_B\left(\frac{\partial C}{\partial y}\frac{\partial T}{\partial y}\right) + \frac{D_T}{T_\infty}\left(\frac{\partial T}{\partial y}\right)^2\right\} + \left(1 + \frac{1}{\beta}\right)\frac{\mu}{\rho c_p}\left(\frac{\partial u}{\partial y}\right)^2, \tag{4}$$

$$u\frac{\partial C}{\partial x} + v\frac{\partial C}{\partial y} = D_B\frac{\partial^2 C}{\partial y^2} + \frac{D_T}{T_\infty}\frac{\partial^2 T}{\partial y^2} - K_0\left(C - C_\infty\right), \tag{5}$$

subject to the boundary conditions:

$$\begin{aligned} u &= u_w + \left(1 + \frac{1}{\beta}\right)N\rho\nu\frac{\partial u}{\partial y}, \\ v &= 0, \\ T &= T_w + K_1\frac{\partial T}{\partial y}, \\ C &= C_w + K_2\frac{\partial C}{\partial y} \\ &\qquad \text{at } y = 0, \\ u &= 0, \\ T &= T_\infty, \\ C &= C_\infty \\ &\qquad \text{as } y \longrightarrow \infty, \end{aligned} \tag{6}$$

where u and v are the velocity components along the x- and y-axes, respectively, ρ_f is the density of base fluid, ν is the kinematic viscosity of the base fluid, $\alpha = k/\rho c_p$ is the thermal diffusivity of the base fluid, $\tau = (\rho c)_p/(\rho c)_f$ is the ratio of nanoparticle heat capacity and the base fluid heat capacity, D_B is the Brownian diffusion coefficient, and D_T is the thermophoretic diffusion coefficient. Furthermore, N, K_1, and K_2 are velocity, thermal, and concentration slip factor. The following nondimensional variables are defined as

$$\begin{aligned} \eta &= \left(\frac{b}{\nu}\right)^{1/2} y, \\ \psi(x, y) &= (b\nu)^{1/2} x f(\eta), \\ \theta(\eta) &= \frac{T - T_\infty}{T_w - T_\infty}, \\ \phi(\eta) &= \frac{C - C_\infty}{C_w - C_\infty}. \end{aligned} \tag{7}$$

The continuity equation (2) is satisfied by introducing the stream function $\psi(x, y)$ such that

$$\begin{aligned} u &= \frac{\partial \psi}{\partial y}, \\ v &= -\frac{\partial \psi}{\partial x}. \end{aligned} \tag{8}$$

In view of the above-mentioned transformations, (3)–(6) are reduced to

$$\left(1+\frac{1}{\beta}\right)f'''+ff''-f'^2=0, \tag{9}$$

$$\frac{1}{\Pr}\theta''+f\theta'+Nb\phi'\theta'+Nt\theta'^2+\left(1+\frac{1}{\beta}\right)\mathrm{Ec}f''^2=0, \tag{10}$$

$$\phi''+\mathrm{Le}f\phi'+\frac{Nt}{Nb}\theta''-\mathrm{Le}\chi\phi=0, \tag{11}$$

$$\begin{aligned}
&f(0)=0,\\
&f'(0)=1+\lambda\left(1+\frac{1}{\beta}\right)f''(0),\\
&\theta(0)=1+\gamma\theta'(0),\\
&\phi(0)=1+\delta\phi'(0),\\
&f'(\infty)=0,\\
&\theta(\infty)=0,\\
&\phi(\infty)=0.
\end{aligned} \tag{12}$$

Here prime denotes differentiation with respect to η, f is similarity function, θ is the dimensionless temperature, ϕ is the dimensionless nanoparticle volume fraction, $\Pr = \nu/\alpha$ is Prandtl number, $\mathrm{Le} = \nu/D_B$ is Lewis number, $\gamma = K_1(b/\nu)^{1/2}$ is the thermal slip parameter, $\beta = \mu_B\sqrt{2\pi_c}/p_y$ is the Casson parameter, $\lambda = N\rho(\nu b)^{1/2}$ is the slip parameter, $\delta = K_2(b/\nu)^{1/2}$ is the concentration slip parameter, $\mathrm{Ec} = u_w^2/c_p(T_w - T_\infty)$ is the Eckert number, $\chi = K_0/b$ is the chemical reaction parameter, $Nb = (\rho c)_p D_B(C_w - C_\infty)/(\rho c)_f\nu$ is the Brownian motion parameter, and $Nt = (\rho c)_p D_T(T_w - T_\infty)/(\rho c)_f\nu T_\infty$ is the thermophoresis parameter, respectively. It should be mentioned here that ($\chi > 0$) indicates a destructive chemical reaction while ($\chi < 0$) corresponds to a generative chemical reaction. The quantities of physical interest in this problem are the local skin friction coefficient, C_{fx}, the local Nusselt number, Nu_x, and local Sherwood number, Sh_x, which are defined as

$$\begin{aligned}
C_{fx}&=\frac{\tau_w}{\rho u_w^2},\\
\mathrm{Nu}_x&=\frac{xq_w}{k(T_w-T_\infty)},\\
\mathrm{Sh}_x&=\frac{xq_m}{D_B(C_w-C_\infty)},
\end{aligned} \tag{13}$$

where τ_w is the shear stress and q_w and q_m are, respectively, the surface heat and mass flux which are given by the following expressions:

$$\begin{aligned}
\tau_w&=\left(\mu_B+\frac{p_y}{\sqrt{2\pi_c}}\right)\left(\frac{\partial u}{\partial y}\right)_{y=0},\\
q_w&=-k\left(\frac{\partial T}{\partial y}\right)_{y=0},\\
q_m&=-D_B\left(\frac{\partial C}{\partial y}\right)_{y=0}.
\end{aligned} \tag{14}$$

The dimensionless forms of skin friction, the local Nusselt number, and the local Sherwood number become

$$\begin{aligned}
\mathrm{Re}_x^{1/2}C_f&=\left(1+\frac{1}{\beta}\right)f''(0),\\
\frac{\mathrm{Nu}_x}{\mathrm{Re}_x^{1/2}}&=-\theta'(0),\\
\frac{\mathrm{Sh}_x}{\mathrm{Re}_x^{1/2}}&=-\phi'(0),
\end{aligned} \tag{15}$$

where $\mathrm{Re}_x = xu_w/\nu$ is the local Reynolds number.

3. Numerical Procedure

The nonlinear differential equations (9)–(11) along with the boundary conditions (12) constitute a two-point boundary value problem (BVP) and they are solved numerically using shooting method, by converting them into an initial value problem (IVP). In this method, the system of (9)–(11) is reduced to the following system of first-order ordinary differential equations:

$$\begin{aligned}
f'&=p,\\
p'&=q,\\
q'&=\left(\frac{\beta}{1+\beta}\right)\left[p^2-fq\right],\\
\theta'&=z,\\
\phi'&=s,\\
z'&=-\Pr\left(fz+Nbsz+Ntz^2+\left(1+\frac{1}{\beta}\right)\mathrm{Ec}q^2\right),\\
s'&=\mathrm{Le}(\chi\phi-fs)-\frac{Nt}{Nb}z'
\end{aligned} \tag{16}$$

with the initial conditions

$$\begin{aligned}
&f(0)=0,\\
&p(0)=1+\lambda\left(1+\frac{1}{\beta}\right)q(0),\\
&\theta(0)=1+\gamma z(0),\\
&\phi(0)=1+\delta s(0).
\end{aligned} \tag{17}$$

The initial guess values of $q(0)$, that is, $f''(0)$, $z(0)$, that is, $\theta'(0)$, and $s(0)$, that is, $\phi'(0)$, are chosen, and the initial value problem (16)-(17) is solved repeatedly by using fourth-order Runge-Kutta method. Then the calculated values of $f'(\eta)$, $\theta(\eta)$, and $\phi(\eta)$ at $\eta_\infty(=8)$ are compared with the given boundary conditions $f'(\eta_\infty) = 0$, $\theta(\eta_\infty) = 0$, and $\phi(\eta_\infty) = 0$, and the values of $f''(0)$, $\theta'(0)$, and $\phi'(0)$ are adjusted by "secant method" to give a better approximation for the solution. The step size is taken as $\Delta\eta = 0.001$. A convergence criterion based on the relative difference between the

Table 1: Comparison of results for $-\theta'(0)$ with different values of Pr, when $\beta \to \infty$ and $\mathrm{Ec} = \delta = \chi = \gamma = \lambda = N = Nt = \mathrm{Le} = 0$.

Pr	$-\theta'(0)$ Khan and Pop [10]	$-\theta'(0)$ Makinde and Aziz [12]	$-\theta'(0)$ Alsaedi et al. [45]	$-\theta'(0)$ Abolbashari et al. [41]	$-\theta'(0)$ Present results
0.07	0.0663	0.0656	0.0663	—	0.0662
0.20	0.1691	0.1691	0.1691	0.1691	0.1691
0.70	0.4539	0.4539	0.4539	0.4539	0.4538
2.0	0.9113	0.9114	0.9113	0.9114	0.9113
7.0	1.8954	1.8954	—	1.8954	1.8954

Table 2: Comparison of results for $-\theta'(0)$ and $-\phi'(0)$ with Nb and Nt for $\beta \to \infty$, $\mathrm{Ec} = \delta = \chi = \gamma = \lambda = 0$, and $\mathrm{Le} = \mathrm{Pr} = 10$.

Nb	Nt	$-\theta'(0)$ Noghrehabadi et al. [46]	$-\theta'(0)$ Present results	$-\phi'(0)$ Noghrehabadi et al. [46]	$-\phi'(0)$ Present results
0.1	0.1	0.952377	0.952376	2.129394	2.129389
	0.3	0.520079	0.520079	2.528638	2.528635
	0.5	0.321054	0.321054	3.035142	3.035144
0.2	0.1	0.505581	0.505581	2.381871	2.381876
	0.3	0.273096	0.273096	2.655459	2.655457
	0.5	0.168077	0.168077	2.888339	2.888336
0.3	0.1	0.252156	0.252156	2.410019	2.410015
	0.3	0.135514	0.135514	2.608819	2.608817
	0.5	0.083298	0.083298	2.751875	2.751873

Table 3: Comparison of results for $-\theta'(0)$ and $-\varphi'(0)$ with Nb and Nt for $\beta \to \infty$, $\mathrm{Ec} = \delta = \chi = \gamma = 0$, $\lambda = 0.5$, and $\mathrm{Le} = \mathrm{Pr} = 10$.

Nb	Nt	$-\theta'(0)$ Noghrehabadi et al. [46]	$-\theta'(0)$ Present results	$-\phi'(0)$ Noghrehabadi et al. [46]	$-\phi'(0)$ Present results
0.1	0.1	0.799317	0.799310	1.787171	1.787142
	0.3	0.436495	0.436492	2.122251	2.122243
	0.5	0.269457	0.269454	2.547353	2.547347
0.2	0.1	0.424328	0.424324	1.99907	1.99904
	0.3	0.229206	0.229204	2.228691	2.228688
	0.5	0.141064	0.141061	2.424144	2.424139
0.3	0.1	0.211631	0.211630	2.022696	2.022672
	0.3	0.113735	0.113731	2.189547	2.189539
	0.5	0.069911	0.069921	2.309612	2.309609

current and previous iteration values is employed. When the difference reaches less than 10^{-6}, the solution is assumed to converge and the iterative process is terminated. Tables 1–3 ensure the validation of the present numerical solutions with the previous literature. It is observed that the obtained results are in excellent agreement with the published work [10, 12, 41, 45, 46]. Numerical calculations were performed in the ranges $0.3 \le \beta \le \infty$, $0 \le \lambda \le 3$, $0 \le \gamma < 4$, $0 \le \delta \le 3$, $0.1 \le Nt \le 0.6$, $0.1 \le Nb \le 0.6$, $1 \le \mathrm{Pr} \le 10$, $-0.3 \le \chi \le 0.5$, and $1 \le \mathrm{Le} \le 10$ with $0.1 \le \mathrm{Ec} \le 1$.

4. Results and Discussions

The nonlinear ordinary differential equations (9)–(11) subject to the boundary conditions (12) are solved numerically by using a shooting method with the fourth-order Runge-Kutta integration scheme. For various physical parameters, the numerical values of the friction factor (in terms of the wall velocity gradient, $f''(0)$), Nusselt number (in terms of heat transfer rate, $-\theta'(0)$), and local Sherwood number (in terms of mass transfer rate, $-\phi'(0)$) are shown in Tables 4 and 5, for both cases of Newtonian ($\beta \to \infty$) and non-Newtonian flows. From Table 4, it is seen that the magnitude of the friction factor and the heat and mass transfer rates reduce with an increase in the slip parameter, λ. Physically, the presence of a slip parameter generates a resistive force adjacent to a stretching surface which diminishes the friction factor and heat and mass transfer rates. One can observe that the heat transfer rate reduces with an increase in the thermal slip parameter, γ, whereas the opposite results effect is seen in the mass transfer rate. Additionally, it is noticed that the heat transfer rate is enhanced with an increase in concentration slip parameter, δ, whereas the opposite results effect is seen in the mass transfer rate. It is clear that the

Table 4: Numerical values of $(1 + 1/\beta) f''(0)$, $-\theta'(0)$, and $-\phi'(0)$ with λ, γ, δ, and β for $Nt = Nb = 0.1$, Ec $= \chi = 0.2$, Pr = 4, and Le = 5.

λ	γ	δ	β	$(1 + 1/\beta) f''(0)$	$-\theta'(0)$	$-\phi'(0)$
0	0.2	0.2	0.5	−1.733110	0.628232	1.3244
1	0.2	0.2	0.5	−0.541057	0.587859	1.0473
3	0.2	0.2	0.5	−0.243961	0.473596	0.972528
0.2	**0**	0.2	0.5	−1.164996	0.76304	1.17273
0.2	**1**	0.2	0.5	−1.164996	0.411102	1.24197
0.2	**3**	0.2	0.5	−1.164996	0.208327	1.28847
0.2	0.2	**0**	0.5	−1.164996	0.620139	1.63936
0.2	0.2	**1**	0.5	−1.164996	0.707216	0.569352
0.2	0.2	**3**	0.5	−1.164996	0.734532	0.246761
0.2	0.2	0.2	**0.3**	−1.319520	0.651801	1.18842
0.2	0.2	0.2	**4**	−0.846526	0.655087	1.18529
0.2	0.2	0.2	∞	−0.776388	0.652042	1.17971

Table 5: Numerical values of $-\theta'(0)$ and $-\phi'(0)$ with Nt, Nb, χ, and Ec for $\lambda = \gamma = \delta = 0.2$, $\beta = 0.5$, Pr = 4, and Le = 5.

Nt	Nb	χ	Ec	$-\theta'(0)$	$-\phi'(0)$
0.1	0.1	0.2	0.2	0.655854	1.19213
0.3	0.1	0.2	0.2	0.510010	1.22598
0.5	0.1	0.2	0.2	0.394448	1.45703
0.1	**0.2**	0.2	0.2	0.550359	1.27665
0.1	**0.4**	0.2	0.2	0.371446	1.31245
0.1	**0.6**	0.2	0.2	0.235575	1.31891
0.1	0.1	**−0.2**	0.2	0.664530	0.637467
0.1	0.1	**0.0**	0.2	0.659002	0.961861
0.1	0.1	**0.4**	0.2	0.654009	1.367830
0.1	0.1	0.2	**0.0**	0.795783	1.113521
0.1	0.1	0.2	**1.0**	0.082093	1.515737
0.1	0.1	0.2	**1.3**	−0.139103	1.641030

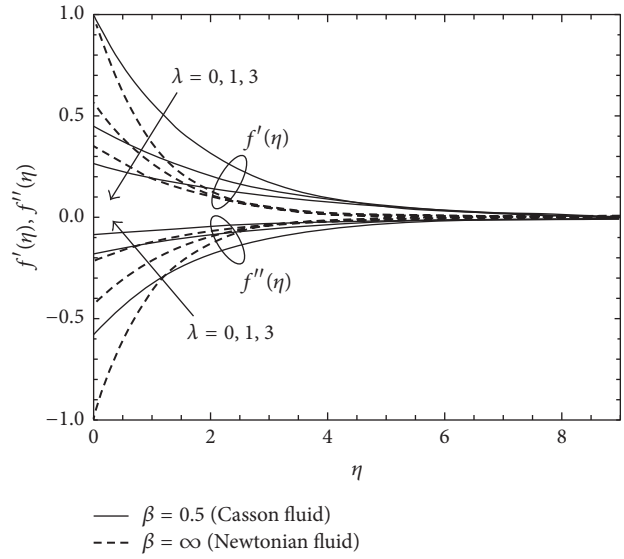

Figure 2: Velocity profile and skin friction coefficient for various values of β and λ.

magnitude of the friction factor and the mass transfer rate diminish with an increase in Casson parameter, β. For the non-Newtonian nanofluid case ($0.3 \leq \beta \leq 4$), the heat transfer rate is enhanced, whereas the opposite results hold with the Newtonian nanofluid case ($\beta \to \infty$). From Table 5, it is also noticed that the heat transfer rate diminishes with an increase in Brownian motion, Nb, and thermophoresis parameter, Nt. Physically, the presence of solid nanoparticles within the conventional working fluid generates a force normal to the imposed temperature gradient which is defined as thermophoretic force. This force has the tendency to move the nanoparticles of high thermal conductivity towards the cold fluid at the ambient. This causes an increase in the temperature of the fluid, but on the contrary, the heat transfer rate reduces within the thermal boundary layer as shown in Figure 9. On the other hand, the mass transfer rate augments with an increase in Brownian motion, Nb, and thermophoresis parameter, Nt. These results are identical to those declared by Khan and Pop [10]. In addition, the heat transfer rate is boosted with generative chemical reaction case ($\chi \prec 0$) whereas the opposite results hold with destructive chemical reaction case ($\chi \succ 0$). With destructive chemical reaction case ($\chi \succ 0$), the mass transfer rate is enhanced, whereas the opposite results hold with generative chemical reaction case ($\chi \prec 0$). It is noticed that the heat transfer reduces with increasing Eckert number, Ec, whereas the reverse trend is seen in the mass transfer. Physically, the presence of Eckert number produces viscous heating which decreases the heat transfer rate at the moving plate surface. Figures 2–18 are drawn in order to see the influence of slip parameter, λ, thermal slip parameter, γ, concentration slip parameter, δ, Brownian motion parameter, Nb, thermophoresis parameter, Nt, chemical reaction parameter, χ, and Eckert number, Ec, on the velocity, the temperature, and the nanoparticle concentration distributions for both cases of Newtonian and non-Newtonian fluids, respectively. The influences of the slip parameter, λ, on the velocity, $f'(\eta)$, the magnitude of the skin friction coefficient, $f''(0)$, the temperature, $\theta(\eta)$, and the nanoparticle concentration profiles, $\phi(\eta)$, are shown in Figures 2–4. It is noted from Figures 2–4 that the velocity

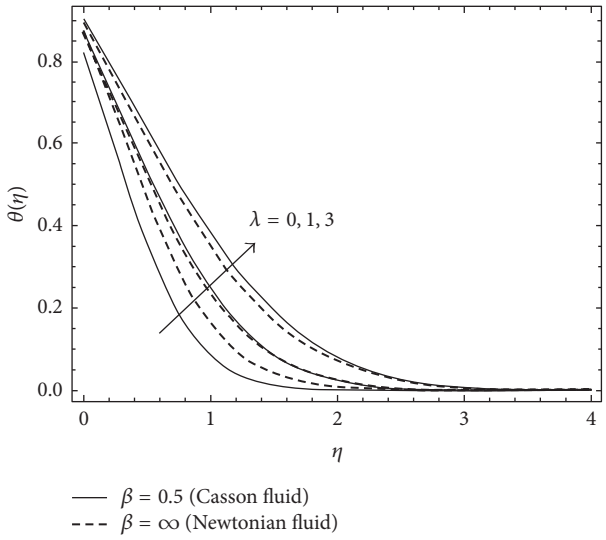

Figure 3: Temperature profile for various values of β and λ.

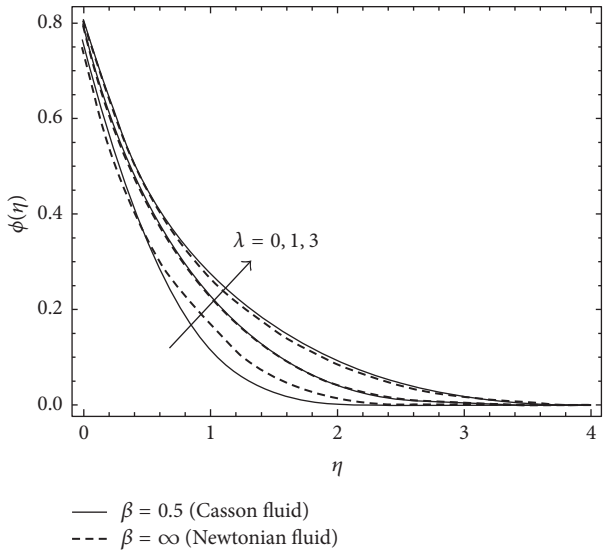

Figure 4: Nanoparticle concentration profile for various values of β and λ.

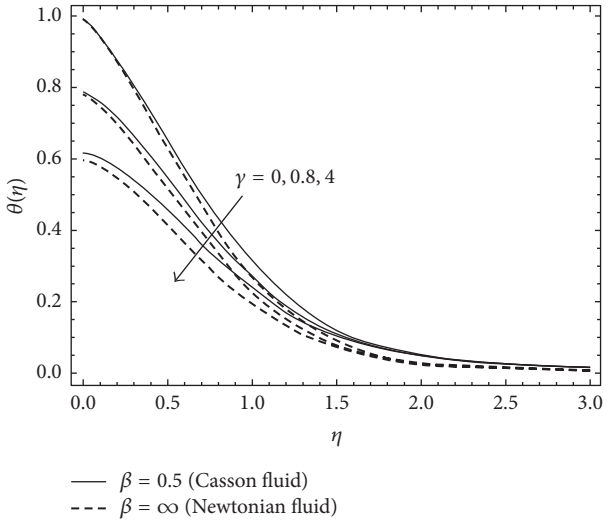

Figure 5: Temperature profile for various values of β and γ.

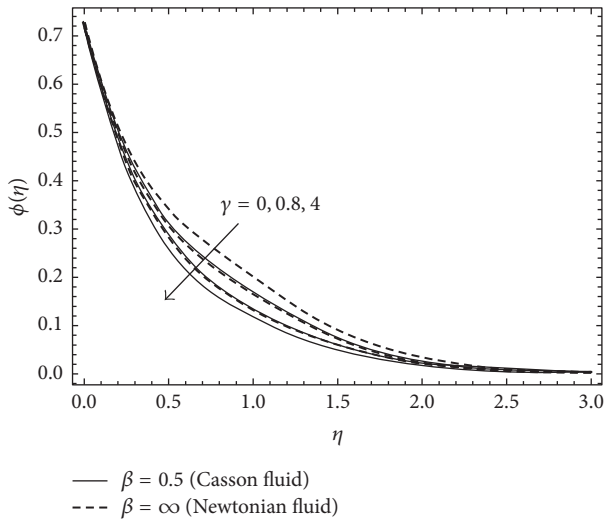

Figure 6: Nanoparticle concentration profile for various values of β and γ.

profile and the magnitude of the skin friction coefficient reduce with an increase in slip parameter, whereas the reverse trend is seen for temperature and nanoparticle concentration profiles. This is due to the fact that a rise in slip parameter, λ, causes a decrease in the surface skin friction between the stretching sheet and the fluid. On the other hand, an increase in the slip factor generates the friction force which allows more fluid to slip past the sheet and the flow decelerating, and the temperature and the nanoparticle concentration fields are enhanced owing to the occurrence of the force. For non-Newtonian fluids, the impact of slip factor is more pronounced in comparison with the Newtonian flow. These results are similar to those reported by Noghrehabadi et al. [46]. Figures 5 and 6 depict the impacts of the thermal slip parameter, γ, on the temperature, and the nanoparticle concentration distributions. It is found from Figures 5 and 6 that the temperature and the nanoparticle concentration distributions reduce with an increase in the thermal slip parameter. Physically, an increase in the thermal slip parameter leads to diminishing the heat transfer inside the boundary layer regime. The temperature distribution for non-Newtonian fluid is more pronounced for all values of γ than Newtonian fluid. The concentration distribution of Newtonian fluid is more pronounced for all values of γ than non-Newtonian fluid. Figures 7 and 8 illustrate the effects of the concentration slip parameter, δ, on the temperature and the nanoparticle concentration profiles. It is observed from Figures 7 and 8 that the temperature and nanoparticle concentration profiles reduce with an increase in concentration slip parameter. The temperature profile for non-Newtonian fluid is more

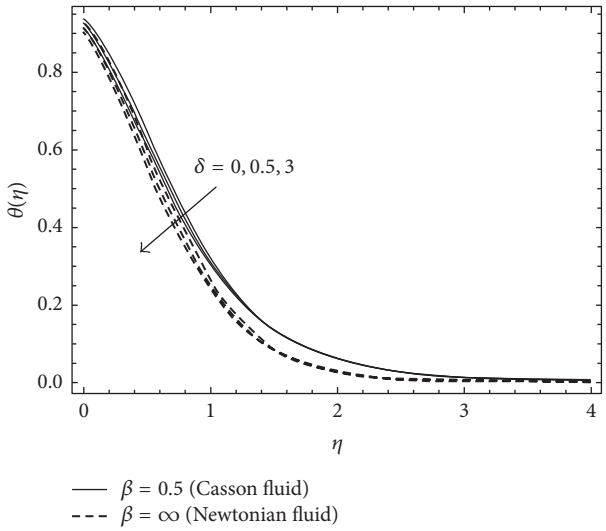

Figure 7: Temperature profile for various values of β and δ.

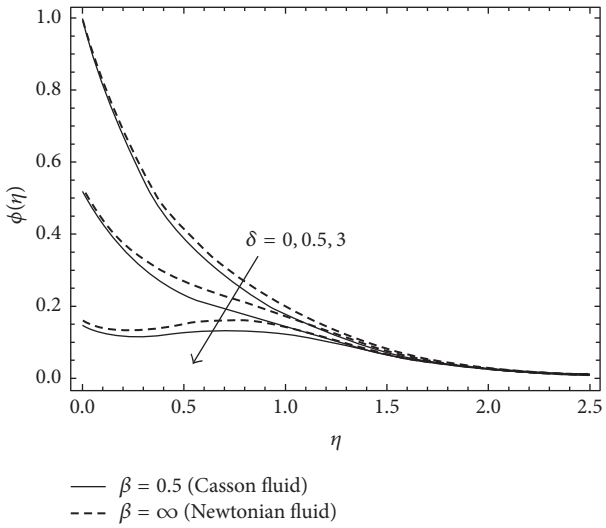

Figure 8: Nanoparticle concentration profile for various values of β and δ.

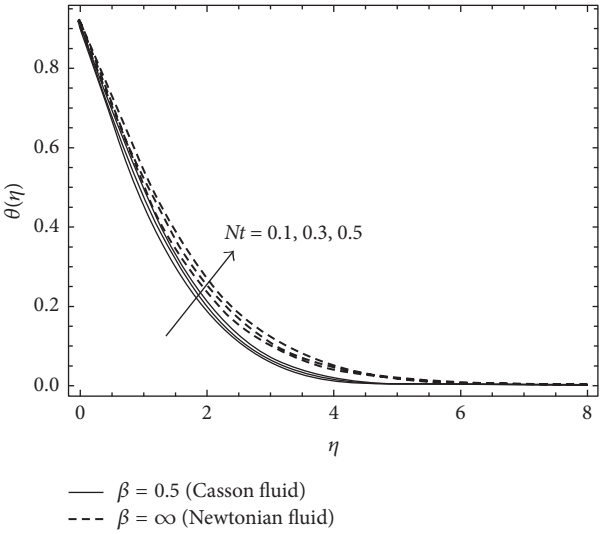

Figure 9: Temperature profile for various values of β and Nt.

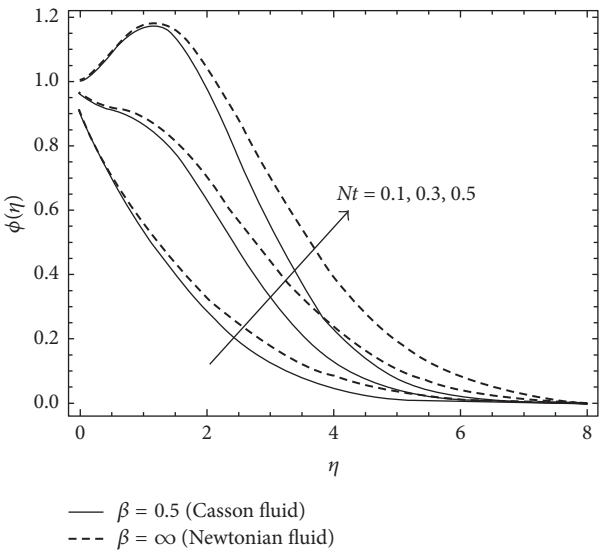

Figure 10: Nanoparticle concentration profile for various values of β and Nt.

pronounced with a rise in δ than Newtonian fluid. The nanoparticle concentration in the case of Newtonian flow is higher than that of non-Newtonian fluid for all values of δ. The influences of the thermophoresis parameter, Nt, on the temperature and the concentration fields are displayed in Figures 9 and 10. It is observed that the temperature and the nanoparticle concentration fields are enhanced with an increase in thermophoresis parameter. Physically, an increase in the thermophoresis parameter leads to an increase in the thermophoretic force inside a fluid regime, which causes an enhancement of the temperature and nanoparticle concentration fields. It is found that the increment in the temperature and the nanoparticle concentration fields for Newtonian fluid due to thermophoresis parameter is higher than that of non-Newtonian fluid. Figures 11 and 12 present the impacts of the Brownian motion parameter, Nb, on the temperature and the concentration distributions. It is noticed that the temperature distribution augments with an increase in the Brownian motion parameter, whereas the reverse trend is observed for the concentration profile. Physically, the increase in Brownian motion helps to warm the boundary layer which tends to move nanoparticles from the stretching sheet to the quiescent fluid. Hence the concentration nanoparticle reduces. It is easily noticeable that the temperature and concentration distributions of Newtonian fluid are more pronounced for all values of Nb than non-Newtonian fluid. The effects of the thermophoresis parameter, Nt, Brownian motion parameter, Nb, and chemical reaction parameter, χ, on the concentration profile for a non-Newtonian fluid are presented in Figures 13 and 14. It is noticed from Figures 13 and 14 that the concentration profile diminishes with an

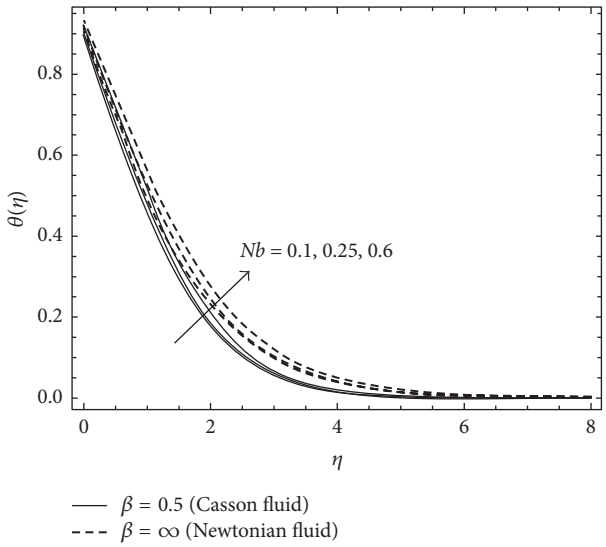

Figure 11: Temperature profile for various values of β and Nb.

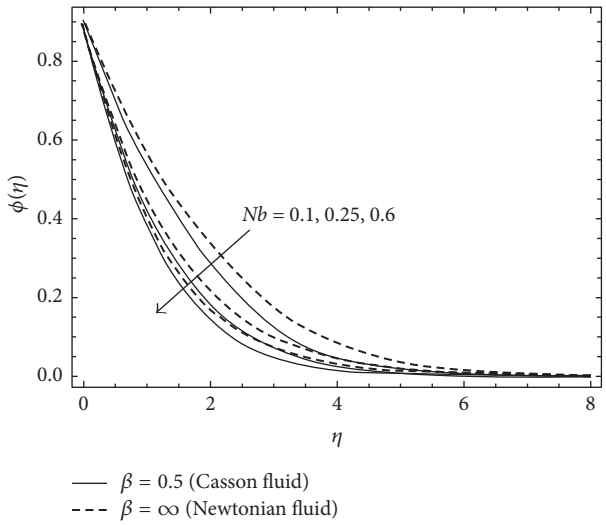

Figure 12: Nanoparticle concentration profile for various values of β and Nb.

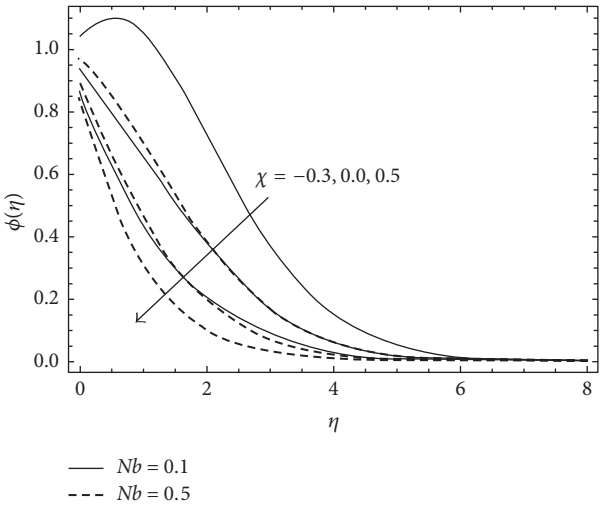

Figure 13: Nanoparticle concentration profile for various values of χ and Nb.

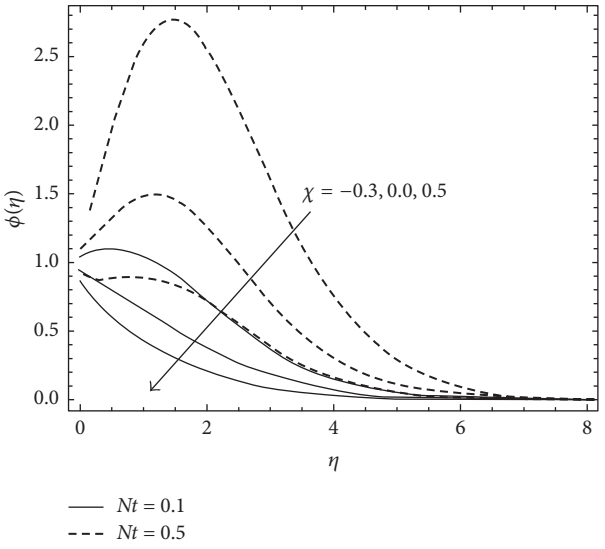

Figure 14: Nanoparticle concentration profile for various values of χ and Nt.

increase in the chemical reaction parameter. It is also noticed that nanoparticle concentration and concentration boundary layer thickness increase with the generative chemical reaction case ($\chi < 0$) whereas the reverse trend is observed in the destructive chemical reaction case ($\chi > 0$). Physically, the presence of a destructive case ($\chi > 0$) causes the transformation of the species as a reason of chemical reaction which decreases the concentration distribution in the concentration boundary layer thickness. For generative chemical reaction case ($\chi < 0$), a generative chemical reaction is illustrated, that is, the species which diffuses from the stretching sheet in the free stream and thereby augments the concentration in the concentration boundary layer thickness. It is observed that the concentration field reduces with an increase in the Brownian motion parameter, Nb, whereas the opposite trend is noticed with thermophoresis parameter, Nt. Figures 15 and 16 elucidate the influences of the thermophoresis parameter, Nt, Brownian motion parameter, Nb, and Lewis number, Le, on the nanoparticle concentration profile for a non-Newtonian fluid. It is observed from Figures 15 and 16 that the concentration distribution augments with an increase in thermophoresis parameter, whereas the reverse trend is observed with an increase in the Brownian motion parameter for all values of Lewis number. On the other hand, the concentration profile diminishes with an increase in Lewis number. Physically, Lewis number is the ratio of momentum diffusivity to Brownian diffusion coefficient. Increasing Lewis number leads to a decrease in the Brownian diffusion coefficient, which causes a reduction in the concentration field. The impact of the Eckert number on the temperature and the concentration fields for both cases is plotted in Figures 17 and 18.

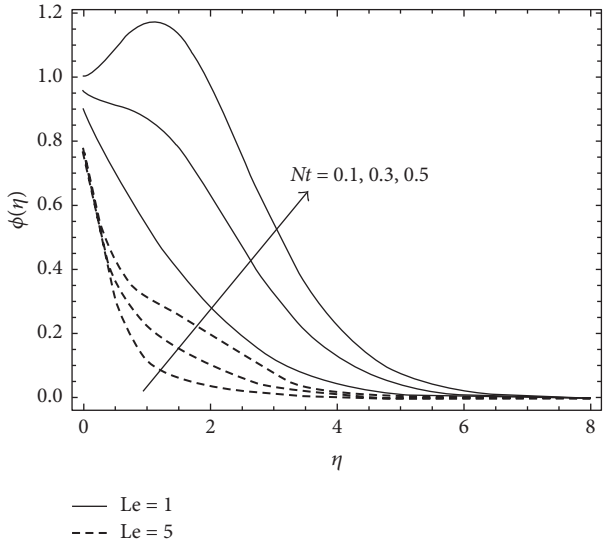

Figure 15: Nanoparticle concentration profile for various values of Le and Nt.

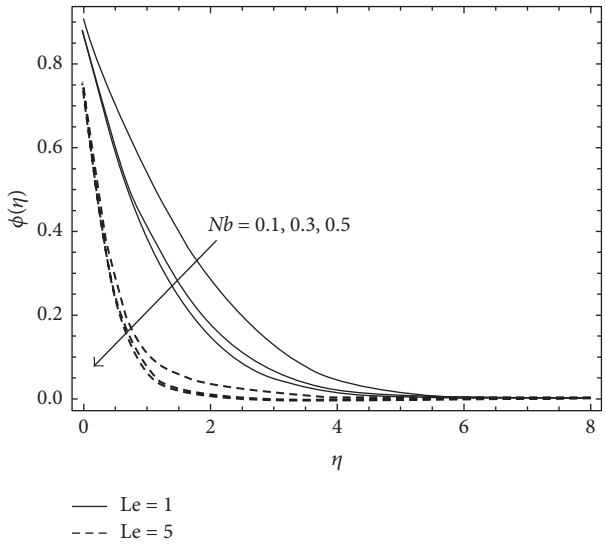

Figure 16: Nanoparticle concentration profile for various values of Le and Nb.

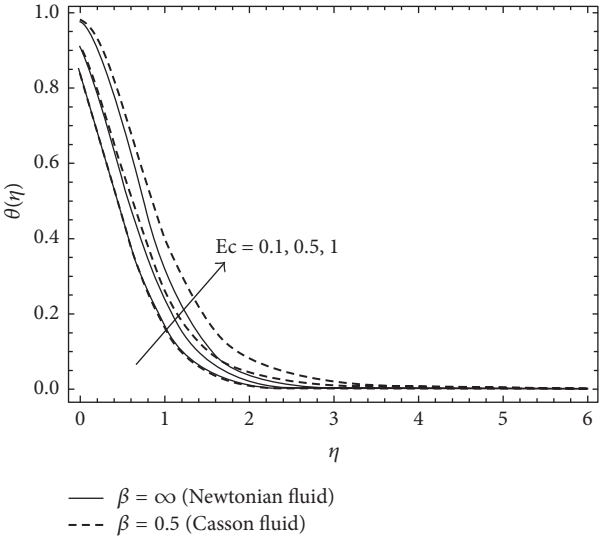

Figure 17: Temperature profile for various values of Ec and β.

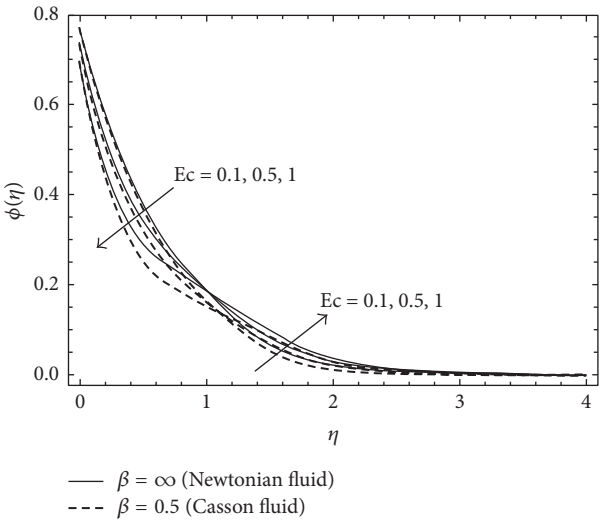

Figure 18: Nanoparticle concentration profile for various values of Ec and β.

It is found from Figure 17 that the temperature field is enhanced with an increase in Eckert number. Physically, Eckert number is the ratio of kinetic energy to enthalpy. Therefore, an increase in Eckert number causes an increase in thermal energy which in turn enhances the temperature and thermal boundary layer thickness of nanofluid. This agrees with the fact that the heat transfer rate at the surface decreases with an increase in Eckert number as shown in Table 5. It is also noticed from Figure 18 that the concentration distribution reduces with an increase in Eckert number near the surface, whereas the reverse trend is observed far away from the surface in both cases.

5. Conclusions

The steady boundary layer flow of Casson nanofluid over a stretching surface with chemical reaction, slip boundary conditions, and viscous dissipation has been numerically studied. The effects of various parameters on velocity, temperature, and nanoparticle concentration fields as well as the friction factor, the heat transfer, and the mass transfer rates are discussed through graphs and tables. The validity of the present analysis is established by comparing the existing results with previously published data. The main conclusions emerging from this study are as follows:

(1) The heat transfer rate is augmented whereas the mass transfer rate is clearly decreased with generative chemical reaction case.

(2) The mass transfer rate is elevated, whereas the heat transfer rate is markedly decelerated with the destructive chemical reaction case.

(3) The magnitudes of the friction factor, the heat transfer, and the mass transfer rates are reduced with an increase in slip parameter.

(4) The heat transfer rate is diminished, whereas the opposite effect is found in the mass transfer rate with an increase in the thermal slip parameter.

(5) The heat transfer rate is augmented whereas the mass transfer rate is considerably reduced with a rise in concentration slip parameter.

(6) The heat transfer rate is decreased whereas the mass transfer rate is distinctly boosted with an increase in Brownian motion and thermophoresis parameter.

(7) The heat transfer rate is reduced, whereas the mass transfer rate is enhanced with an increase in Eckert number.

(8) The magnitudes of the friction factor and the mass transfer rate are enhanced with an increase in the Casson parameter in both cases.

(9) The heat transfer rate is enhanced in the non-Newtonian nanofluid case, whereas the opposite influence is noticed in the Newtonian nanofluid case.

(10) The nanoparticle concentration distribution is enhanced with the generative chemical reaction, whereas the opposite influence is noticed with the destructive chemical reaction.

Conflicts of Interest

The author declares that there are no conflicts of interest regarding the publication of this paper.

References

[1] S. U. S. Choi, "Enhancing thermal conductivity of fluids with nanoparticles," in *Proceedings of the in Proceedings of the 1995 ASME International Mechanical Engineering Congress and Exposition*, vol. 66, pp. 99–105, San Francisco, Calif, USA, 1995.

[2] S. Lee, S. U. Choi, S. Li, and J. A. Eastman, "Measuring thermal conductivity of fluids containing oxide nanoparticles," *Journal of Heat Transfer*, vol. 121, no. 2, pp. 280–289, 1999.

[3] J. A. Eastman, S. U. S. Choi, S. Li, W. Yu, and L. J. Thompson, "Anomalously increased effective thermal conductivities of ethylene glycol-based nanofluids containing copper nanoparticles," *Applied Physics Letters*, vol. 78, no. 6, pp. 718–720, 2001.

[4] H. Ş. Aybar, M. Sharifpur, M. R. Azizian, M. Mehrabi, and J. P. Meyer, "A review of thermal conductivity models for nanofluids," *Heat Transfer Engineering*, vol. 36, no. 13, pp. 1085–1110, 2015.

[5] X. Wang, X. Xu, and S. U. S. Choi, "Thermal conductivity of nanoparticle-fluid mixture," *Journal of Thermophysics and Heat Transfer*, vol. 13, no. 4, pp. 474–480, 1999.

[6] A. A. Afify and M. A. A. Bazid, "Flow and heat transfer analysis of nanofluids over a moving surface with temperature-dependent viscosity and viscous dissipation," *Journal of Computational and Theoretical Nanoscience*, vol. 11, no. 12, pp. 2440–2448, 2014.

[7] Y. Lin, B. Li, L. Zheng, and G. Chen, "Particle shape and radiation effects on Marangoni boundary layer flow and heat transfer of copper-water nanofluid driven by an exponential temperature," *Powder Technology*, vol. 301, pp. 379–386, 2016.

[8] J. Buongiorno, "Convective transport in nanofluids," *Journal of Heat Transfer*, vol. 128, no. 3, pp. 240–250, 2006.

[9] D. A. Nield and A. V. Kuznetsov, "Thermal instability in a porous medium layer saturated by a nanofluid," *International Journal of Heat and Mass Transfer*, vol. 52, no. 25-26, pp. 5796–5801, 2009.

[10] W. A. Khan and I. Pop, "Boundary-layer flow of a nanofluid past a stretching sheet," *International Journal of Heat and Mass Transfer*, vol. 53, no. 11-12, pp. 2477–2483, 2010.

[11] D. A. Nield and A. V. Kuznetsov, "The Cheng-Minkowycz problem for the double-diffusive natural convective boundary layer flow in a porous medium saturated by a nanofluid," *International Journal of Heat and Mass Transfer*, vol. 54, no. 1–3, pp. 374–378, 2011.

[12] O. D. Makinde and A. Aziz, "Boundary layer flow of a nanofluid past a stretching sheet with a convective boundary condition," *International Journal of Thermal Sciences*, vol. 50, no. 7, pp. 1326–1332, 2011.

[13] P. Rana, R. Bhargava, and O. A. Bég, "Numerical solution for mixed convection boundary layer flow of a nanofluid along an inclined plate embedded in a porous medium," *Computers and Mathematics with Applications*, vol. 64, no. 9, pp. 2816–2832, 2012.

[14] A. A. Afify and M. A. A. Bazid, "Effects of variable fluid properties on the natural convective boundary layer flow of a nanofluid past a vertical plate: numerical study," *Journal of Computational and Theoretical Nanoscience*, vol. 11, no. 1, pp. 210–218, 2014.

[15] O. D. Makinde, F. Mabood, W. A. Khan, and M. S. Tshehla, "MHD flow of a variable viscosity nanofluid over a radially stretching convective surface with radiative heat," *Journal of Molecular Liquids*, vol. 219, pp. 624–630, 2016.

[16] F. M. Hady, F. S. Ibrahim, S. M. Abdel-Gaied, and M. R. Eid, "Boundary-layer non-Newtonian flow over vertical plate in porous medium saturated with nanofluid," *Applied Mathematics and Mechanics*, vol. 32, no. 12, pp. 1577–1586, 2011.

[17] C.-Y. Cheng, "Free convection of non-Newtonian nanofluids about a vertical truncated cone in a porous medium," *International Communications in Heat and Mass Transfer*, vol. 39, no. 9, pp. 1348–1353, 2012.

[18] A. M. Rashad, M. A. El-Hakiem, and M. M. Abdou, "Natural convection boundary layer of a non-Newtonian fluid about a permeable vertical cone embedded in a porous medium saturated with a nanofluid," *Computers and Mathematics with Applications*, vol. 62, pp. 3140–3151, 2011.

[19] M. Ramzan, M. Bilal, J. D. Chung, and U. Farooq, "Mixed convective flow of Maxwell nanofluid past a porous vertical stretched surface—An optimal solution," *Results in Physics*, vol. 6, pp. 1072–1079, 2016.

[20] T. Hayat, T. Muhammad, S. A. Shehzad, and A. Alsaedi, "Three-dimensional boundary layer flow of Maxwell nanofluid: mathematical model," *Applied Mathematics and Mechanics*, vol. 36, no. 6, pp. 747–762, 2015.

[21] M. Y. Abou-Zeid, "Homotopy perturbation method to gliding motion of bacteria on a layer of power-law nanoslime with heat transfer," *Journal of Computational and Theoretical Nanoscience*, vol. 12, no. 10, pp. 3605–3614, 2015.

[22] M. Y. Abou-Zeid, "Effects of thermal-diffusion and viscous dissipation on peristaltic flow of micropolar non-Newtonian nanofluid: application of homotopy perturbation method," *Results in Physics*, vol. 6, pp. 481–495, 2016.

[23] R. Ellahi, "The effects of MHD and temperature dependent viscosity on the flow of non-Newtonian nanofluid in a pipe: analytical solutions," *Applied Mathematical Modelling*, vol. 37, no. 3, pp. 1451–1467, 2013.

[24] M. Y. Abou-Zeid, A. A. Shaaban, and M. Y. Alnour, "Numerical treatment and global error estimation of natural convective effects on gliding motion of bacteria on a power-lawnanoslime through a non-darcy porous medium," *Journal of Porous Media*, vol. 18, no. 11, pp. 1091–1106, 2015.

[25] C. S. K. Raju, N. Sandeep, and A. Malvandi, "Free convective heat and mass transfer of MHD non-Newtonian nanofluids over a cone in the presence of non-uniform heat source/sink," *Journal of Molecular Liquids*, vol. 221, pp. 108–115, 2016.

[26] N. Casson, *In Reheology of Dipersed System*, Peragamon Press, Oxford, UK, 1959.

[27] M. Mustafa, T. Hayat, I. Pop, and A. Aziz, "Unsteady boundary layer flow of a Casson fluid due to an impulsively started moving flat plate," *Heat Transfer—Asian Research*, vol. 40, no. 6, pp. 563–576, 2011.

[28] S. Nadeem, R. Mehmood, and N. S. Akbar, "Optimized analytical solution for oblique flow of a Casson-nano fluid with convective boundary conditions," *International Journal of Thermal Sciences*, vol. 78, pp. 90–100, 2014.

[29] G. Makanda, S. Shaw, and P. Sibanda, "Diffusion of chemically reactive species in Casson fluid flow over an unsteady stretching surface in porous medium in the presence of a magnetic field," *Mathematical Problems in Engineering*, vol. 2015, Article ID 724596, 10 pages, 2015.

[30] T. Hayat, S. Asad, and A. Alsaedi, "Flow of Casson fluid with nanoparticles," *Applied Mathematics and Mechanics*, vol. 37, no. 4, pp. 459–470, 2016.

[31] K. Das, P. R. Duari, and P. K. Kundu, "Numerical simulation of nanofluid flow with convective boundary condition," *Journal of the Egyptian Mathematical Society*, vol. 23, no. 2, pp. 435–439, 2015.

[32] M. Abd El-Aziz, "Effect of time-dependent chemical reaction on stagnation point flow and heat transfer over a stretching sheet in a nanofluid," *Physica Scripta*, vol. 89, no. 8, Article ID 085205, 2014.

[33] N. T. M. El-Dabe, A. A. Shaaban, M. Y. Abou-Zeid, and H. A. Ali, "Magnetohydrodynamic non-Newtonian nanofluid flow over a stretching sheet through a non-Darcy porous medium with radiation and chemical reaction," *Journal of Computational and Theoretical Nanoscience*, vol. 12, no. 12, pp. 5363–5371, 2015.

[34] M. R. Eid, "Chemical reaction effect on MHD boundary-layer flow of two-phase nanofluid model over an exponentially stretching sheet with a heat generation," *Journal of Molecular Liquids*, vol. 220, pp. 718–725, 2016.

[35] A. A. Afify and N. S. Elgazery, "Effect of a chemical reaction on magnetohydrodynamic boundary layer flow of a Maxwell fluid over a stretching sheet with nanoparticles," *Particuology*, vol. 29, pp. 154–161, 2016.

[36] C. L. M. H. Navier, "Mémoire sur les lois du mouvement des fluides," *Mémoires de Académie Royale des Sciences de Institut de France*, vol. 6, pp. 389–440, 1823.

[37] A. Rashad, "Unsteady nanofluid flow over an inclined stretching surface with convective boundary condition and anisotropic slip impact," *International Journal of Heat and Technology*, vol. 35, no. 1, pp. 82–90, 2017.

[38] A. A. Afify, M. J. Uddin, and M. Ferdows, "Scaling group transformation for MHD boundary layer flow over permeable stretching sheet in presence of slip flow with Newtonian heating effects," *Applied Mathematics and Mechanics*, vol. 35, no. 11, pp. 1375–1386, 2014.

[39] S. M. M. El-Kabeir, E. R. El-Zahar, and A. M. Rashad, "Effect of chemical reaction on heat and mass transfer by mixed convection flow of casson fluid about a sphere with partial slip," *Journal of Computational and Theoretical Nanoscience*, vol. 13, no. 8, pp. 5218–5226, 2016.

[40] A. A. Afify, "Slip effects on the flow and heat transfer of nanofluids over an unsteady stretching surface with heat generation/absorption," *Journal of Computational and Theoretical Nanoscience*, vol. 12, no. 3, pp. 484–491, 2015.

[41] M. H. Abolbashari, N. Freidoonimehr, F. Nazari, and M. M. Rashidi, "Analytical modeling of entropy generation for Casson nano-fluid flow induced by a stretching surface," *Advanced Powder Technology*, vol. 26, no. 2, pp. 542–552, 2015.

[42] M. J. Uddin, W. A. Khan, and A. I. M. Ismail, "Effect of variable properties, Navier slip and convective heating on hydromagnetic transport phenomena," *Indian Journal of Physics*, vol. 90, no. 6, pp. 627–637, 2016.

[43] N. T. M. Eldabe and M. G. E. Salwa, "Heat transfer of MHD non-Newtonian Casson fluid flow between two rotating cylinders," *Journal of the Physical*, vol. 64, pp. 41–64, 1995.

[44] R. U. Haq, S. Nadeem, Z. H. Khan, and T. G. Okedayo, "Convective heat transfer and MHD effects on Casson nanofluid flow over a shrinking sheet," *Central European Journal of Physics*, vol. 12, no. 12, pp. 862–871, 2014.

[45] A. Alsaedi, M. Awais, and T. Hayat, "Effects of heat generation/absorption on stagnation point flow of nanofluid over a surface with convective boundary conditions," *Communications in Nonlinear Science and Numerical Simulation*, vol. 17, no. 11, pp. 4210–4223, 2012.

[46] A. Noghrehabadi, R. Pourrajab, and M. Ghalambaz, "Effect of partial slip boundary condition on the flow and heat transfer of nanofluids past stretching sheet prescribed constant wall temperature," *International Journal of Thermal Sciences*, vol. 54, pp. 253–261, 2012.